

CURRENT NOISE IN QUANTUM POINT CONTACTS

L. DICARLO ^a, YIMING ZHANG ^a, D. T. McCLURE ^a, D. J. REILLY, C. M. MARCUS
Department of Physics, Harvard University, Cambridge, Massachusetts 02138, USA

L. N. PFEIFFER, K. W. WEST
Alcatel-Lucent, Murray Hill, NJ 07974, USA

M. P. HANSON, A. C. GOSSARD
Department of Materials, University of California, Santa Barbara, California 93106, USA

We present measurements of current noise in quantum point contacts as a function of source-drain bias, gate voltage, and in-plane magnetic field. At zero bias, Johnson noise provides a measure of the electron temperature. At finite bias, shot noise at zero field exhibits an asymmetry related to the 0.7 structure in conductance. The asymmetry in noise evolves smoothly into the symmetric signature of spin-resolved electron transmission at high field. Comparison to a phenomenological model with density-dependent level splitting yields quantitative agreement. Additionally, a device-specific contribution to the finite-bias noise, particularly visible on conductance plateaus (where shot noise vanishes), agrees quantitatively with a model of bias-dependent electron heating.

The experimental discovery nearly two decades ago^{1,2} of quantized conductance in quantum point contacts (QPCs) suggested the realization of an electron waveguide. Pioneering measurements^{3,4,5} of noise in QPCs almost a decade later observed suppression of shot noise below the Poissonian value due to Fermi statistics, as predicted by mesoscopic scattering theory^{6,7}. Shot noise has since been increasingly recognized as an important probe of quantum statistics and many-body effects^{8,9}, complementing dc transport. For example, shot-noise measurements have been exploited to directly observe quasiparticle charge in strongly correlated systems^{10,11,12}, as well as to study interacting localized states in mesoscopic tunnel junctions¹³ and cotunneling¹⁴ and dynamical channel blockade^{15,16} in quantum dots.

Paralleling these developments, a large literature has emerged concerning the appearance of an additional plateau-like feature in transport through a QPC at zero magnetic field, termed 0.7 structure. Experiment^{17,18,19,20,21,22} and theory^{23,24,25,26,27,28} suggest that 0.7 structure is a many-body spin effect. Its underlying microscopic origin remains an outstanding problem in mesoscopic physics. This persistently unresolved issue is remarkable given the simplicity of the device.

In this article, we review our recent results^{29,30} on current noise in quantum point contacts—including shot-noise signatures of 0.7 structure and effects of in-plane field B_{\parallel} —and present new results on a device-specific contribution to noise that is well described by a model that includes bias-dependent heating in the vicinity of the QPC. Notably, we observe suppression of shot noise relative to that predicted by theory for spin-degenerate transport^{6,7} near $0.7 \times 2e^2/h$ at $B_{\parallel} = 0$,

^aThese authors contributed equally to this work.

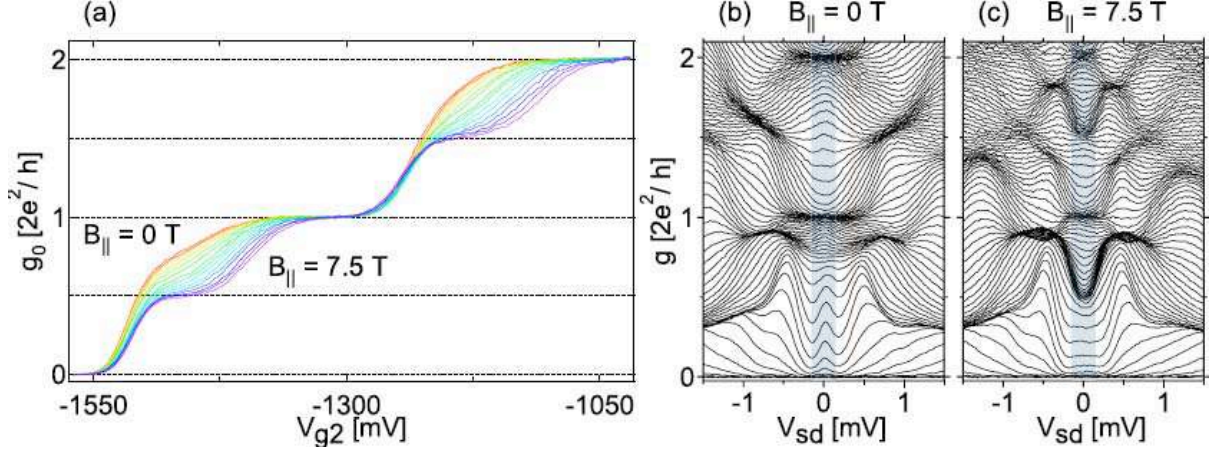


Figure 1: (color) (a) Linear conductance g_0 as a function of V_{g2} ($V_{g1} = -3.2$ V), for B_{\parallel} ranging from 0 (red) to 7.5 T (purple) in steps of 0.5 T. The series resistance R_s ranging from 430 Ω at $B_{\parallel} = 0$ to 730 Ω at $B_{\parallel} = 7.5$ T has been subtracted to align the plateaus at multiples of $2e^2/h$. (b,c) Nonlinear differential conductance g as a function of V_{sd} , at $B_{\parallel} = 0$ (b) and 7.5 T (c), with V_{g2} intervals of 7.5 and 5 mV, respectively. Shaded regions indicate the bias range used for the noise measurements presented in Figs. 3(c) and 4.

consistent with previous work^{31,32}. The suppression near $0.7 \times 2e^2/h$ evolves smoothly with increasing B_{\parallel} into the signature of spin-resolved transmission. We find quantitative agreement between noise data and a phenomenological model for a density-dependent level splitting²⁸, with model parameters extracted solely from conductance. In the final section, we investigate a device-specific contribution to the bias-dependent noise, particularly visible on conductance plateaus (where shot noise vanishes), which we account for with a model⁴ of Wiedemann-Franz thermal conduction in the reservoirs connecting to the QPC.

DC transport

Measurements are presented for two QPCs defined by split gates on GaAs/Al_{0.3}Ga_{0.7}As heterostructures grown by molecular beam epitaxy. For QPC 1(2), the two-dimensional electron gas [2DEG] 190(110) nm below the heterostructure surface has density $1.7(2) \times 10^{11}$ cm⁻² and mobility $5.6(0.2) \times 10^6$ cm²/Vs. Except where noted, all data are taken at the base temperature of a ³He cryostat, with electron temperature T_o of 290 mK. A magnetic field of 125 mT, applied perpendicular to the plane of the 2DEG, was used to reduce bias-dependent heating⁴ (see section below). Each QPC is first characterized at both zero and finite B_{\parallel} using dc transport measurements. The differential conductance $g = dI/dV_{sd}$ (where I is the current and V_{sd} is the source-drain bias) is measured by lock-in technique with an applied $25 \mu V_{rms}$ excitation at 430 Hz³⁰. The B_{\parallel} -dependent ohmic contact and reservoir resistance R_s in series with the QPC is subtracted.

Figure 1 shows conductance data for QPC 1 [see micrograph in Fig. 2(a)]. Linear-response conductance $g_0 = g(V_{sd} \sim 0)$ as a function of gate voltage V_{g2} , for $B_{\parallel} = 0$ to 7.5 T in steps of 0.5 T, is shown in Fig. 1(a). The QPC shows the characteristic quantization of conductance in units of $2e^2/h$ at $B_{\parallel} = 0$, and the appearance of spin-resolved plateaus at multiples of $0.5 \times 2e^2/h$ at $B_{\parallel} = 7.5$ T. Additionally, at $B_{\parallel} = 0$, a shoulder-like 0.7 structure is evident, which evolves continuously into the $0.5 \times 2e^2/h$ spin-resolved plateau at high B_{\parallel} ¹⁷.

Figures 1(b) and 1(c) show g as a function of V_{sd} for evenly spaced V_{g2} settings at $B_{\parallel} = 0$ and 7.5 T, respectively. In this representation, linear-response plateaus in Fig. 1(a) appear as accumulated traces around $V_{sd} \sim 0$ at multiples of $2e^2/h$ for $B_{\parallel} = 0$, and at multiples of $0.5 \times 2e^2/h$ for $B_{\parallel} = 7.5$ T. At finite V_{sd} , additional plateaus occur when a sub-band

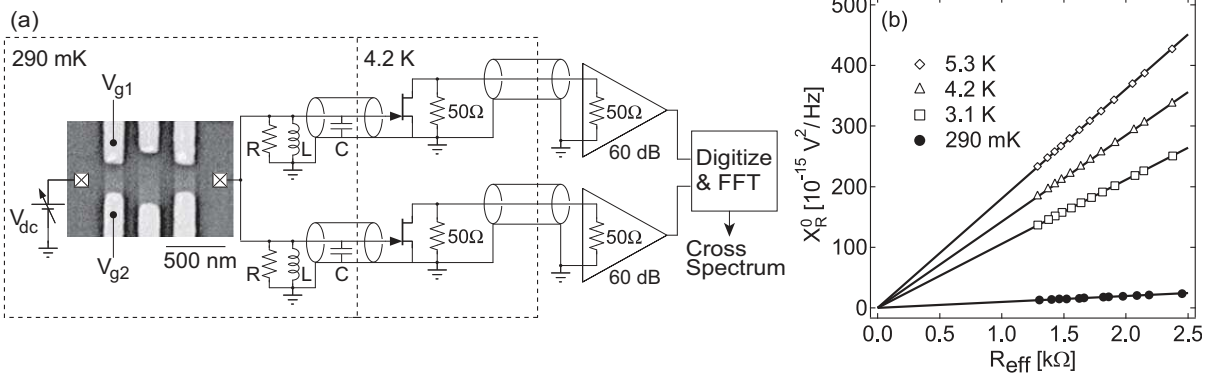


Figure 2: (a) Equivalent circuit near 2 MHz of the system measuring QPC noise by cross-correlation on two amplification channels³⁰. The scanning electron micrograph shows a device of identical design to QPC 1. The QPC is formed by negative voltages V_{g1} and V_{g2} applied on two facing electrostatic gates. All other gates on the device are grounded. (b) Calibration by Johnson noise thermometry of the electron temperature T_o and the cross-correlation gain G_X . X_R^0 as a function of R_{eff} , at base (solid circles) and at three elevated fridge temperatures (open markers). Solid lines are linear fits constrained to the origin. The best-fit slopes at the three elevated temperatures give $G_X = 790$ V/V. Combining this value of G_X with the best-fit slope at base gives $T_o = 290$ mK.

edge lies between the source and drain chemical potentials³³. The features near $0.8 \times 2e^2/h$ ($V_{\text{sd}} \sim \pm 750 \mu\text{V}$) at $B_{\parallel} = 0$ cannot be explained within a single-particle picture³⁵. These features are related to the 0.7 structure around $V_{\text{sd}} \sim 0$ and resemble the spin-resolved finite bias plateaus at $\sim 0.8 \times 2e^2/h$ for $B_{\parallel} = 7.5$ T^{19,20}.

Current noise

The QPC current noise is measured using a cross-correlation technique to suppress amplifier voltage noise³⁰ [see Fig. 2(a)]. Two parallel channels amplify the voltage fluctuations across a resistor-inductor-capacitor resonator that performs current-to-voltage conversion near the resonant frequency of 2 MHz. Each channel consists of a transconductance stage using a high electron mobility transistor (HEMT) cooled to 4.2 K, followed by 50Ω amplification at room temperature. The amplified noise signals from both channels are sampled simultaneously by a digitizer, and their cross-spectral density calculated by fast-Fourier-transform.

Thermal noise and calibration

Measurement of Johnson (thermal) noise allows calibration of T_o and the geometric mean G_X of the voltage gain in the amplification channels, both needed to extract bias-dependent QPC noise. The calibration procedure illustrated in Fig. 2(b) stems from the relation $X_R^0 = G_X^2 \cdot 4k_B T_o R_{\text{eff}}$ valid at $V_{\text{sd}} = 0$, where X_R^0 is the cross-spectral density on resonance and R_{eff} is the effective resistance from the HEMT gates to ground. R_{eff} is measured from the half-power bandwidth of the cross-spectral density³⁰. At elevated refrigerator temperatures 3 – 5 K, where electrons are well thermalized to a calibrated thermometer, a measurement of X_R^0 as a function of R_{eff} (tuned through V_{g2}) allows a calibration of G_X , which is found to be 790 V/V. This value of G_X is then used to determine $T_o = 290$ mK from the same measurement at base temperature.

Bias-dependent noise

To characterize QPC noise at finite bias, we define the excess noise, $S_I^{\text{P}}(V_{\text{sd}}) = S_I(V_{\text{sd}}) - 4k_B T_o g(V_{\text{sd}})$, where S_I is the total QPC current noise spectral density. Note that S_I^{P} is the noise in excess of $4k_B T_o g(V_{\text{sd}})$ rather than $4k_B T_o g(0)$ and thus differs from excess noise as

discussed in Refs. 3 and 32. In the absence of $1/f$ and telegraph noise as well as bias-dependent electron heating, S_I^P originates from the electron partitioning at the QPC.

Experimental values for S_I^P are extracted from simultaneous measurements of X_R^0 , g and R_{eff} using the relation

$$X_R^0 = G_X^2 \left(S_I^P \left(\frac{R_{\text{eff}}}{1 + gR_s} \right)^2 + 4k_B T_o R_{\text{eff}} \right). \quad (1)$$

With an integration time of 60 s, the resolution in S_I^P is 1.4×10^{-29} A²/Hz, corresponding to full shot noise $2eI$ of $I \sim 40$ pA. S_I^P as a function of dc current I for QPC 1 with gates set to very low conductance ($g_0 \sim 0.04 \times 2e^2/h$) [Fig. 3(b)] exhibits full shot noise, $S_I^P = 2e|I|$, demonstrating an absence of $1/f$ and telegraph noise at the noise measurement frequency³⁴.

Figure 3(c) shows $S_I^P(V_{\text{sd}})$ in the V_{sd} range $-150 \mu\text{V}$ to $+150 \mu\text{V}$ [shaded regions in Figs. 1(b) and 1(c)], at $B_{\parallel} = 0$ and V_{g2} settings corresponding to open markers in Fig. 3(a). Similar to when the QPC is fully pinched off, S_I^P vanishes on plateaus of linear conductance. This demonstrates that bias-dependent electron heating is not significant in QPC 1. In contrast, for $g \sim 0.5$ and $1.5 \times 2e^2/h$, S_I^P grows with $|V_{\text{sd}}|$ and shows a transition from quadratic to linear dependence^{3,4,5}. The linear dependence of S_I^P on V_{sd} at high bias further demonstrates the absence of noise due to resistance fluctuations. Solid curves superimposed on the $S_I^P(V_{\text{sd}})$ data in Fig. 3(c) are best-fits to the form

$$S_I^P(V_{\text{sd}}) = 2 \frac{2e^2}{h} \mathcal{N} \left[eV_{\text{sd}} \coth \left(\frac{eV_{\text{sd}}}{2k_B T_o} \right) - 2k_B T_o \right], \quad (2)$$

with the *noise factor* \mathcal{N} as the only free fitting parameter. Note that \mathcal{N} relates S_I^P to V_{sd} , in contrast to the Fano factor^{8,9}, which relates S_I^P to I . This fitting function is motivated by mesoscopic scattering theory^{6,7,8,9}, where transport is described by transmission coefficients $\tau_{n,\sigma}$ (n is the transverse mode index and σ denotes spin) and partition noise originates from the partial transmission of incident electrons. Within scattering theory, the full expression for S_I^P is

$$S_I^P(V_{\text{sd}}) = \frac{2e^2}{h} \int \sum_{n,\sigma} \tau_{n,\sigma}(\varepsilon) (1 - \tau_{n,\sigma}(\varepsilon)) (f_s - f_d)^2 d\varepsilon, \quad (3)$$

where $f_{s(d)}$ is the Fermi function in the source (drain) lead. Equation (2) follows from Eq. (3) only for the case of constant transmission across the energy window of transport, with $\mathcal{N} =$

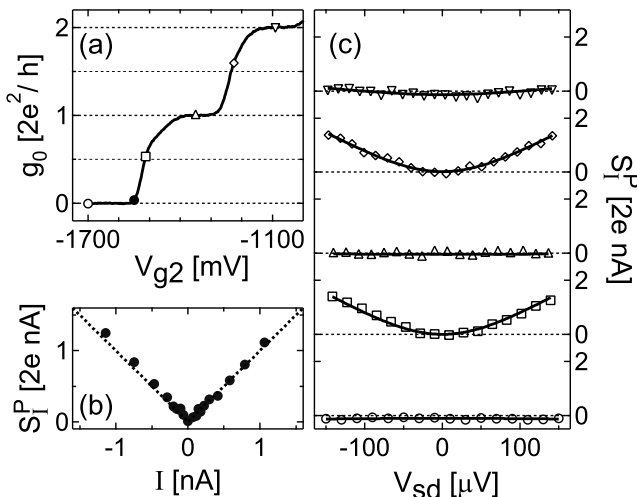


Figure 3: (a) Linear conductance g_0 as a function of V_{g2} at $B_{\parallel} = 0$. Markers indicate V_{g2} settings for the noise measurements shown in (b) and (c). (b) S_I^P as a function of dc current I with the QPC near pinch-off. The dotted line indicates full shot noise $S_I^P = 2e|I|$. (c) Measured S_I^P as a function of V_{sd} , for conductances near 0 (circles), 0.5 (squares), 1 (upward triangles), 1.5 (squares), and $2 \times 2e^2/h$ (downward triangles). Solid lines are best-fits to Eq. (2) using \mathcal{N} as the only fitting parameter. In order of increasing conductance, best-fit \mathcal{N} values are 0.00, 0.20, 0.00, 0.19, and 0.03.

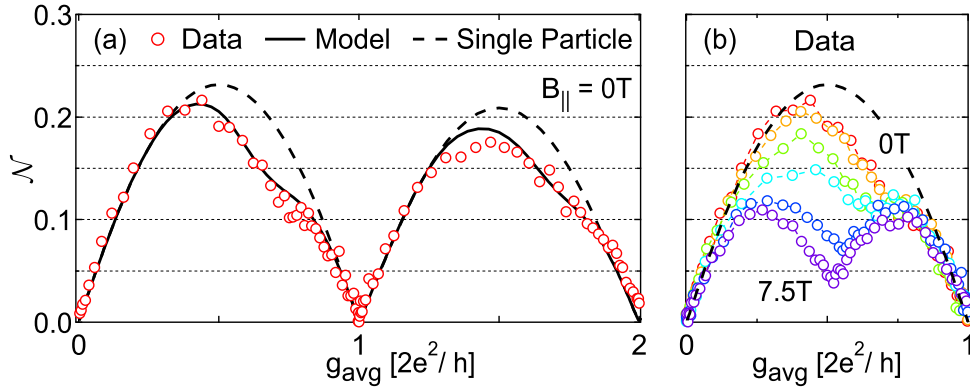


Figure 4: (color) (a) Experimental \mathcal{N} as a function of g_{avg} at $B_{\parallel} = 0$ (red circles) along with model curves for nonzero (solid) and zero (dashed) proportionality of splitting, γ_n (see text). (b) Experimental \mathcal{N} as a function of g_{avg} in the range $0 - 1 \times 2e^2/h$, at $B_{\parallel} = 0$ T (red), 2 T (orange), 3 T (green), 4 T (cyan), 6 T (blue), and 7.5 T (purple). The dashed curve shows the single-particle model ($\gamma_n = 0$) at zero field for comparison.

$\frac{1}{2} \sum \tau_{n,\sigma}(1 - \tau_{n,\sigma})$. Furthermore, for spin-degenerate transmission, \mathcal{N} vanishes at multiples of $2e^2/h$ and reaches the maximal value 0.25 at odd multiples of $0.5 \times 2e^2/h$. Energy dependence of transmission can reduce the maximal value below 0.25, as discussed below.

While Eq. (2) is motivated by scattering theory, the value of \mathcal{N} extracted from fitting to Eq. (2) simply provides a way to quantify $S_I^P(V_{\text{sd}})$ experimentally for each V_{g2} . We have chosen the bias range $e|V_{\text{sd}}| \lesssim 5k_B T_o$ for fitting \mathcal{N} to minimize nonlinear-transport effects while extending beyond the quadratic-to-linear crossover in noise that occurs on the scale $e|V_{\text{sd}}| \sim 2k_B T_o$.

The dependence of \mathcal{N} on conductance at $B_{\parallel} = 0$ is shown in Fig. 4(a), where \mathcal{N} is extracted from measured $S_I^P(V_{\text{sd}})$ at 90 values of V_{g2} . The horizontal axis, g_{avg} , is the average of the differential conductance over the bias points where noise was measured. \mathcal{N} has the shape of a dome, reaching a maximum near odd multiples of $0.5 \times 2e^2/h$ and vanishing at multiples of $2e^2/h$. The observed $\mathcal{N}(g_{\text{avg}})$ deviates from the spin-degenerate, energy-independent scattering theory in two ways. First, there is a reduction in the maximum amplitude of \mathcal{N} below 0.25. Second, there is an asymmetry in \mathcal{N} with respect to $0.5 \times 2e^2/h$, resulting from a noise reduction near the 0.7 feature. A similar but weaker asymmetry is observed about $1.5 \times 2e^2/h$. The reduction in the maximum amplitude can be understood as resulting from an energy dependence of transmissions $\tau_{n,\sigma}$; the asymmetry is a signature of 0.7 structure, as we now discuss.

0.7 structure

We investigate further the relation between the asymmetry in \mathcal{N} and the 0.7 structure by measuring the dependence of $\mathcal{N}(g_{\text{avg}})$ on B_{\parallel} . As shown in Fig. 4(b), \mathcal{N} evolves smoothly from a single asymmetric dome at $B_{\parallel} = 0$ to a symmetric double dome at 7.5 T. The latter is a signature of spin-resolved electron transmission. Notably, for g_{avg} between 0.7 and 1 (in units of $2e^2/h$), \mathcal{N} is insensitive to B_{\parallel} , in contrast to the dependence of \mathcal{N} near $0.3 \times 2e^2/h$.

We compare these experimental data to the shot-noise prediction of a phenomenological model²⁸ for the 0.7 anomaly. This model, originally motivated by dc transport data, assumes a lifting of the twofold spin degeneracy of mode n by an energy splitting $\Delta\varepsilon_{n,\sigma} = \sigma \cdot \rho_n \cdot \gamma_n$ that grows linearly with 1D density ρ_n (with proportionality γ_n) within that mode. Here, $\sigma = \pm 1$ and $\rho_n = \sqrt{2m^*/h} \sum_{\sigma} (\sqrt{\mu_s - \varepsilon_{n,\sigma}} + \sqrt{\mu_d - \varepsilon_{n,\sigma}})$, where $\mu_{s(d)}$ is the source(drain) chemical potential and m^* is the electron effective mass. Parameters of the phenomenological model are extracted

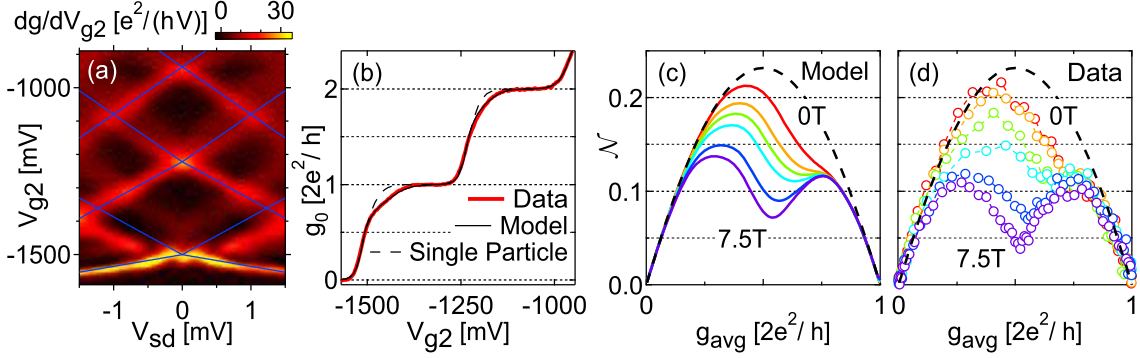


Figure 5: (color) (a) Transconductance dg/dV_{g2} as a function of V_{sd} and V_{g2} . Blue lines trace the alignment of mode edges with source and drain chemical potentials; their slope and intersection give the conversion from V_{g2} to energy and the energy spacing between modes, respectively. As two crossing points are observed between the first and second modes (the model attributes this to spin-splitting in the first mode), we take the midpoint as the crossing point for the blue lines. (c) Measured linear conductance (red) as a function of V_{g2} at $B_{||} = 0$, and linear conductance calculated with the model (black solid) with best-fit values for $\omega_{x,n}$ and γ_n . Single-particle model takes $\gamma_n = 0$ (black dashed). (c) Model \mathcal{N} as a function of g_{avg} in the range $0 - 1 \times 2e^2/h$, at $B_{||} = 0, 2, 3, 4, 6,$ and 7.5 T. (d) Same as Fig. 4(b).

solely from conductance. The lever arm converting V_{g2} to energy (and hence ρ_n) as well as the transverse mode spacing are extracted from transconductance (dg/dV_{g2}) data [Fig. 5(a)]³⁵. Using an energy-dependent transmission $\tau_{n,\sigma}(\varepsilon) = 1/(1 + e^{2\pi(\varepsilon_n,\sigma - \varepsilon)/\hbar\omega_{x,n}})$ for a saddle-point potential³⁶, the value $\omega_{x,n}$ (potential curvature parallel to the current) is found by fitting linear conductance below $0.5 \times 2e^2/h$ (below $1.5 \times 2e^2/h$ for the second mode), and γ_n is obtained by fitting above $0.5(1.5) \times 2e^2/h$, where (within the model) the splitting is largest [see Fig. 5(b)]. We find $\hbar\omega_{x,1(2)}$ is $\sim 500(300)$ μeV and $\gamma_{1(2)} \sim 0.012(0.008)$ $e^2/4\pi\epsilon_0$ for the first (second) mode. Note that the splitting $2 \cdot \rho_n \cdot \gamma_n$ is two orders of magnitude smaller than the direct Coulomb energy of electrons spaced by $1/\rho_n$. Using these parameters, $S_I^P(V_{sd})$ is calculated using Eq. (3), and \mathcal{N} is then extracted by fitting $S_I^P(V_{sd})$ to Eq. (2). The calculated values of $\mathcal{N}(g_{avg})$ at $B_{||} = 0$ are shown along with the experimental data in Fig. 4(a). For comparison we include calculation results accounting for energy-dependent transmission without splitting ($\gamma_n = 0$). The overall reduction of \mathcal{N} arises from a variation in transmission across the 150 μV bias window (comparable to $\hbar\omega_x$), and is a single-particle effect. On the other hand, asymmetry of \mathcal{N} about 0.5 and $1.5 \times 2e^2/h$ requires nonzero γ_n .

Magnetic field is included in the model by assuming a g-factor of 0.44 and adding the Zeeman splitting to the density-dependent splitting, maintaining the parameters obtained above. Figure 5(c) shows calculated $\mathcal{N}(g_{avg})$ at $B_{||}$ corresponding to the experimental data, reproduced in Fig. 5(d). Including the magnetic field in quadrature or as a thermally weighted mixture with the intrinsic density-dependent splitting gives essentially indistinguishable results within this model. Model and experiment show comparable evolution of \mathcal{N} with $B_{||}$: the asymmetric dome for $B_{||} = 0$ evolves smoothly into a double dome for 7.5 T, and for conductance $\gtrsim 0.7 \times 2e^2/h$, the curves for all fields overlap closely. Some differences are observed between data and model, particularly for $B_{||} = 7.5$ T. While the experimental double dome is symmetric with respect to the minimum at $0.5 \times 2e^2/h$, the theory curve remains slightly asymmetric with a less-pronounced minimum. We find that setting the g-factor to ~ 0.6 in the model reproduces the measured symmetrical double dome as well as the minimum value of \mathcal{N} at $0.5 \times 2e^2/h$. This observation is consistent with reports of an enhanced g-factor in QPCs at low density^{17,20}.

Recent theoretical treatments of 0.7 structure have also addressed its shot-noise signature. Modelling screening of the Coulomb interaction in the QPC, Lassl *et al.*³⁷ qualitatively re-

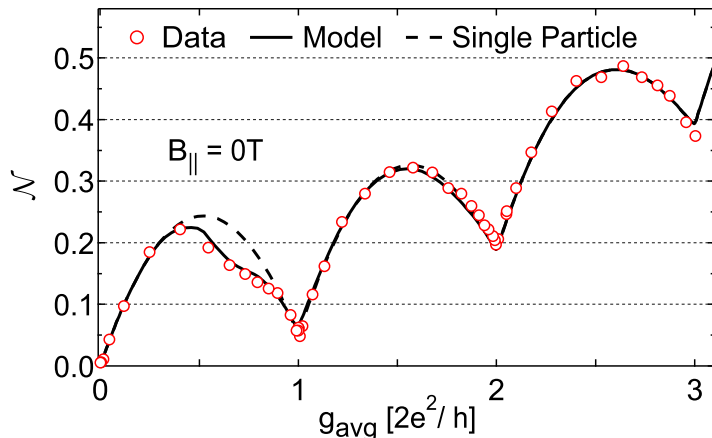


Figure 6: (color) Experimental \mathcal{N} as a function of g_{avg} at $B_{\parallel} = 0$ (red circles) for QPC 2, along with model curves for nonzero (solid) and zero (dashed) proportionality of splitting γ_n . Model calculations include bias-dependent electron heating.

produce the B_{\parallel} -dependent \mathcal{N} . Jaksch *et al.*³⁸ find a density-dependent splitting in density-functional calculations that include exchange and correlation effects. This theory justifies the phenomenological model and is consistent with the observed shot-noise suppression. Using a generalized single-impurity Anderson model motivated by density-functional calculations that suggest a quasi-bound state³⁹, Golub *et al.*⁴⁰ find quantitative agreement with the B_{\parallel} -dependent \mathcal{N} .

Bias-dependent electron heating

In contrast to QPC 1, noise data in QPC 2 show evidence of bias-dependent electron heating. Figure 6 shows $\mathcal{N}(g_{\text{avg}})$ at $B_{\parallel} = 0$ over the first three conductance steps, extracted from fits using Eq. (2) to $S_I^P(V_{\text{sd}})$ data over the range $|V_{\text{sd}}| \leq 400 \mu\text{V}$ at 50 gate voltage settings. As in Fig. 4(a), a clear asymmetry in the noise factor is observed, associated with enhanced noise reduction near $0.7 \times 2e^2/h$. For this device, \mathcal{N} remains finite on conductance plateaus, showing super-linear dependence on plateau index. This is consistent with bias-dependent thermal noise resulting from electron heating. Following Ref. 4, we incorporate into our model the bias-dependent electron temperature $T_e(V_{\text{sd}}) = \sqrt{T_o^2 + (24/\pi^2)(g/g_m)(1 + 2g/g_m)(eV_{\text{sd}}/2k_B)^2}$, where g_m is the parallel conductance of the reservoirs connecting to the QPC. This expression⁴ models diffusion by Wiedemann-Franz thermal conduction of the heat flux $gV_{\text{sd}}^2/2$ on each side of the QPC and of Joule heating in the reservoirs, assuming ohmic contacts thermalized to the lattice at T_o . In the absence of independent measurements of reservoir and ohmic contact resistances, we treat $1/g_m$ as a single free parameter.

Theoretical \mathcal{N} curves including effects of bias-dependent heating are obtained from fits to Eq. (2) of calculated $S_I(V_{\text{sd}}, T_e(V_{\text{sd}})) - 4k_B T_o g(V_{\text{sd}})$. Parameters $\omega_{x,n} = 1.35, 1.13, 0.86 \text{ meV}$ and $\gamma_n = 0.019, 0.008, 0 e^2/4\pi\epsilon_0$ for the first three modes (in increasing order) are extracted from conductance data. To avoid complications arising from a zero-bias anomaly²⁰ present in this device, γ_0 is extracted from the splitting of the first sub-band edge in the transconductance image²⁸, rather than from linear conductance. Other parameters are extracted in the same way as for QPC 1. As shown in Fig. 6, quantitative agreement with the \mathcal{N} data is obtained over the three conductance steps with $1/g_m = 75 \Omega$.

In conclusion, we have presented measurements of current noise in quantum point contacts as a function of source-drain bias, gate voltage, and in-plane magnetic field. We have observed a shot-noise signature of the 0.7 structure at zero field, and investigated its evolution with increasing field into the signature of spin-resolved transmission. Comparison to a phe-

nomenological model with density-dependent level splitting yielded quantitative agreement, and a device-specific contribution to bias-dependent noise was shown to be consistent with electron heating.

Acknowledgments

We thank H.-A. Engel, M. Heiblum, L. Levitov, and A. Yacoby for valuable discussions, and S. K. Slater, E. Onitskansky, N. J. Craig, and J. B. Miller for device fabrication. We acknowledge support from NSF-NSEC, ARO/ARDA/DTO, and Harvard University.

References

1. B. J. van Wees *et al.*, Phys. Rev. Lett. **60**, 848 (1988).
2. D. A. Wharam *et al.*, J. Phys. C **21**, L209 (1988).
3. M. Reznikov *et al.*, Phys. Rev. Lett. **75**, 3340 (1995).
4. A. Kumar *et al.*, Phys. Rev. Lett. **76**, 2778 (1996).
5. R. C. Liu *et al.*, Nature **391**, 263 (1998).
6. G. B. Lesovik, Pis'ma Zh. Eksp. Teor. Fiz. **49**, 513 (1989) [JETP. Lett. **49**, 592 (1989)].
7. M. Büttiker, Phys. Rev. Lett. **65**, 2901 (1990).
8. Ya. M. Blanter and M. Büttiker, Phys. Rep. **336**, 1 (2000); Ya. M. Blanter, cond-mat/0511478.
9. T. Martin in *Nanophysics: Coherence and Transport, Les Houches Session LXXXI*, eds. H. Bouchiat *et al.* (Elsevier, Amsterdam, 2005), cond-mat/0501208.
10. R. de-Picciotto *et al.*, Nature **389**, 162 (1997); M. Reznikov *et al.*, Nature **399**, 238 (1999).
11. L. Saminadayar *et al.*, Phys. Rev. Lett. **79**, 2526 (1997).
12. X. Jehl *et al.*, Nature **405**, 50 (2000).
13. S. S. Safonov *et al.*, Phys. Rev. Lett. **91**, 136801 (2003).
14. E. Onac *et al.*, Phys. Rev. Lett. **96**, 026803 (2006).
15. S. Gustavsson *et al.*, Phys. Rev. B **74**, 195303 (2006).
16. Y. Zhang *et al.*, cond-mat/0703419.
17. K. J. Thomas *et al.*, Phys. Rev. Lett. **77**, 135 (1996).
18. A. Kristensen *et al.*, Phys. Rev. B **62**, 10950 (2000).
19. D. J. Reilly *et al.*, Phys. Rev. B **63**, 121311(R) (2001); D. J. Reilly *et al.*, Phys. Rev. Lett. **89**, 246801 (2002).
20. S. M. Cronenwett *et al.*, Phys. Rev. Lett. **88**, 226805 (2002).
21. W. D. Oliver, Ph.D. Dissertation, Stanford University, 2002.
22. L. P. Rokhinson *et al.*, Phys. Rev. Lett. **96**, 156602 (2006).
23. C. K. Wang and K.-F. Berggren, Phys. Rev. B **54**, 14257(R) (1996).
24. H. Bruus *et al.*, Physica E **10**, 97 (2001).
25. Y. Meir *et al.*, Phys. Rev. Lett. **89**, 196802 (2002).
26. K. A. Matveev, Phys. Rev. Lett. **92**, 106801 (2004).
27. A. Ramšak and J. H. Jefferson, Phys. Rev. B **71**, 161311(R) (2005).
28. D. J. Reilly, Phys. Rev. B **72**, 033309 (2005); D. J. Reilly *et al.*, Physica E **34**, 27 (2006).
29. L. DiCarlo *et al.*, Phys. Rev. Lett. **97**, 036810 (2006).
30. L. DiCarlo *et al.*, Rev. Sci. Instrum. **77**, 073906 (2006).
31. M. Avinun-Kalish *et al.*, Phys. Rev. Lett. **92**, 156801 (2004).
32. P. Roche *et al.*, Phys. Rev. Lett. **93**, 116602 (2004).
33. L. P. Kouwenhoven *et al.*, Phys. Rev. B **39**, 8040(R) (1989).
34. Y. Chen and R. A. Webb, Phys. Rev. B **73**, 035424 (2006).
35. N. K. Patel *et al.*, Phys. Rev. B **44**, 13549 (1991).
36. M. Büttiker, Phys. Rev. B **41**, 7906(R) (1990).
37. A. Lassl *et al.*, Phys. Rev. B **75**, 045346 (2007).
38. P. Jaksch *et al.*, Phys. Rev. B **74**, 235320 (2006).
39. T. Rejec and Y. Meir, Nature **442**, 900 (2006).
40. A. Golub *et al.*, Phys. Rev. Lett. **97**, 186801 (2006).